Synthesis of Carbon-Encapsulated Metal Nanoparticles from Wood Char

Yicheng Du Chuji Wang Hossein Toghiani Zhiyong Cai
Xiaojian Liu Jilei Zhang Qiangu Yan

Abstract

Carbon-encapsulated metal nanoparticles were synthesized by thermal treatment of wood char, with or without transition metal ions pre-impregnated, at 900°C to 1,100°C. Nanoparticles with concentric multilayer shells were observed. The nanoparticles were analyzed by scanning electron microscopy, transmission electron microscopy (TEM), X-ray diffraction (XRD), and energy dispersive X-ray (EDX) spectroscopy. The EDX spectrum showed that carbon was the dominant element in the shells. TEM and XRD analysis indicated that the generated carbon shells had structures similar to that of graphite with an average interplanar distance of 0.34 nm. The effects of temperature and pre-impregnation of metal ions on the yield of carbon-encapsulated metal nanoparticles were studied.

The late 20th century witnessed creation of several synthetic carbon allotropes that differ from naturally occurring forms of carbon. These carbon allotropes include lonsdaleite (Frondel and Marvin 1967), buckminsterfullerene (Kroto et al. 1985), carbon nanofoam discovered by Andrei V. Rode and coworkers in 1997 (cf. Reddy et al. 2009), carbon nanotubes (Iijima 1991), and carbon onions (Ugarte 1995). These single-substance carbon materials have broadened the carbon allotrope family.

In recent years another new type of nanostructured carbon material, carbon-encapsulated metal nanoparticles (CEMNs), has been reported. The CEMNs have a typical core-shell structure of metal cores surrounded by multilayer carbon shells that have an average interplanar distance of 0.34 nm. Because of their unique magnetic and electrical properties and their high thermal and chemical stabilities, these CEMNs have potential value-added applications in magnetic data storage, xerography, electronics, catalysis, and drug delivery (Hsin et al. 2008, Lu et al. 2010). Since the discovery of this new nanomaterial, fabrication and characterization of CEMNs have been increasingly studied.

Current synthesis methods of CEMNs include high-temperature annealing (HTA; Harris and Tsang 1998, Tomita et al. 2000, Kaburagi et al. 2002, Wu et al. 2002, Qiu et al. 2004, Tokoro et al. 2004, Sunny et al. 2010), arc discharge or modified arc discharge (Jiao et al. 1996, Seraphin et al. 1996, Ermoline et al. 2002, Ling et al. 2003, Xu et al. 2006, Liu et al. 2010), chemical vapor deposition (Flahaut et al. 2002, Liu et al. 2002, Wang et al. 2003, El-Gendy et al. 2009, Lu et al. 2010), electron beam irradiation (Nishijo et al. 2005), pyrolysis of organometallic compounds (Sano et al. 2003), microwave arcing (Hsin et al. 2008), and explosion or detonation (Wu et al. 2003, Lu et al. 2005). Detailed discussion of the advantages and limitations of these methods are available in the literature. Among these methods, HTA is identified as a simple and efficient method for high-volume production. To date, carbon sources that have been used in the HTA method for CEMN synthesis include carbon-containing polymers, diamond nanoparticles, pitch, and graphite. Limited study has been reported on the use of wood or annual agricultural biomass as the carbon source. Lian and Wu (2009) conducted the only published study using agricultural materials as the carbon source. In that study, cellulose fibers were impregnated with aqueous salt solutions and carbonized at 180°C to 380°C, and the resultant nanoparticles had metal cores surrounded by amorphous carbon.

Wood is the most common form of biomass. The abundant and low-cost carbon sources from biomass are an easily obtained raw carbon precursor material for value-

The authors are, respectively, Postdoctoral Research Fellow, Faculty of Forestry, Univ. of Toronto, Toronto, Ontario, Canada (yicheng.du@utoronto.ca); Associate Professor, Dept. of Physics and Astronomy (cw175@msstate.edu), and Associate Professor, Dave C. Swalm School of Chemical Engineering (hossein@che.msstate.edu), Mississippi State Univ., Starkville; Project Leader, USDA Forest Serv., Forest Products Lab., Madison, Wisconsin (zcai@fs.fed.us); and Graduate Student, Dept. of Mathematics and Statistics (xl6@msstate.edu), Professor, Dept. of Forest Products (jzhang@cfr.msstate.edu), and Postdoctoral Research Associate, Ag & Bio Engineering (qy8@ra.msstate.edu), Mississippi State Univ., Starkville. Approved for publication as Journal Article no. FP574 of the Forest and Wildlife Research Center, Mississippi State University. This paper was received for publication in September 2010. Article no. 10-00041.

Forest Prod. J. 60(6):527–533.

added carbonaceous nanoparticle production. Fast pyrolysis of wood for bio-oil production has been extensively investigated in recent years because of the excess consumption of fossil fuels. Wood char is a by-product from the fast pyrolysis of wood, and it accounts for 15 to 25 percent (by weight) of total products (Mohan et al. 2006). The high cost of manufacture is one of the hindrances for the commercialization of bio-oil production. The utilization of wood char for fabricating CEMNs will provide added value for this by-product and eventually help improve the wood pyrolysis process economics. In this study, the use of wood char as the raw material and selected metals as precursors to synthesize CEMNs was examined. The objective of this work was to demonstrate the feasibility of using an alternative raw material for CEMN synthesis through a cost-effective thermal-treatment method.

Materials and Methods

Materials

Wood char particles used in this study were provided by the Forest Products Bio-oil Laboratory at Mississippi State University. The wood char particles were derived from the fast pyrolysis of southern yellow pine chips using an auger reactor. Southern yellow pine mainly consists of C, H, and O, and trace inorganic elements (Koch 1972). Figure 1 shows the wood char particles used in the present work. Iron nitrate and nickel nitrate 1,000-ppm (1-mg/mL) standard solutions were purchased from EM Science (Gibbstown, New Jersey) and Absolute Standards, Inc. (Hamden, Connecticut), respectively. Iron nitrate nonahydrate and nickel nitrate hexahydrate were purchased from Fisher Scientific, Inc. All chemicals were ACS reagent grade and were used as received.

Metal ion pre-impregnation

Iron nitrate and nickel nitrate solutions were used to bathe the wood char for the purpose of improving the production yield. The solution number, concentration, and measured pH value of each solution are summarized in Table 1. The wood char particles were impregnated with iron or nickel nitrate salt by immersion in these standard 1,000-ppm or as-prepared 10 percent (wt/wt) aqueous solutions for 24 hours, respectively. After being soaked in these solutions, the wood char particles were dried at 103°C for 24 hours. Control wood char particles without ion pretreatment were also prepared for comparison purposes.

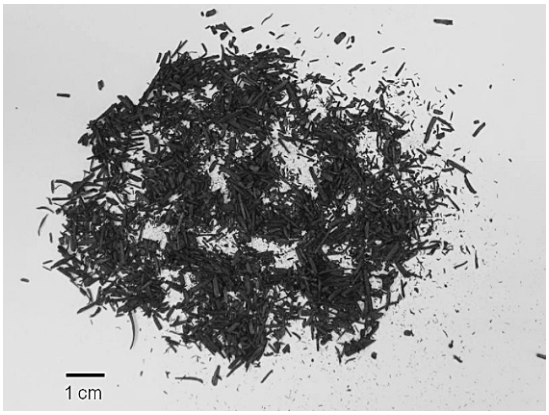

Figure 1.—Wood char particles, a by-product from fast pyrolysis of southern yellow pine chips.

Table 1.—Standard and prepared iron nitrate and nickel nitrate solutions.

Solution no.	Solution	Concentration	Measured pH value
1	Fe: 1,000 ppm	Fe: 1 mg/mL	1.17
2	Ni: 1,000 ppm	Ni: 1 mg/mL	1.07
3	Iron nitrate in de-ionized water	$Fe(NO_3)_3$: 10% (wt/wt)	0.98
4	Nickel nitrate in de-ionized water	$Ni(NO_3)_2$: 10% (wt/wt)	3.60

Thermal treatment

Control or Fe^{3+}- and Ni^{2+}-impregnated wood char particles (2 to 3 g) were placed in a quartz tube inserted into a split furnace (Mellen SC12R-0.75X3). The furnace was equipped with a temperature controller (Mellen PS 305-120-15-S1). Control samples and samples pre-impregnated with metal ions were heated to 900°C to 1,100°C at a ramping rate of 20°C/min in a flowing argon atmosphere (1 liter/min). After the furnace was held at the desired temperature for 1 hour, the furnace was turned off and the samples were allowed to cool to ambient temperature naturally. The sample number, pre-impregnation solution, and corresponding treatment temperature and duration are summarized in Table 2. The experimental setup schematic for the thermal-treatment process is illustrated in Figure 2.

Characterization

Specimens for scanning electron microscopy (SEM) observation were mounted on aluminum stubs with carbon tape and coated with gold-palladium in a Polaron E 5100 Sputter Coater for 30 seconds. SEM images were taken on a JSM-6500F field emission SEM. The wood char samples for transmission electron microscopy (TEM) and X-ray diffraction (XRD) studies were ground into powder form using an agate mortar and pestle set. XRD samples were prepared

Table 2.—Sample number with corresponding treatment.

	Treatment		
	Metal ion impregnation	Thermal treatment	
Sample no.	Solution no.	Temperature (°C)	Duration (h)
Control			
A	No	No	No
B	No	900	1
C	No	1,000	1
D	No	1,100	1
Standard solutions			
E	1	No	No
F	1	1,000	1
G	2	No	No
H	2	1,000	1
Prepared solutions			
I	3	No	No
J	3	1,000	1
K	4	No	No
L	4	1,000	1

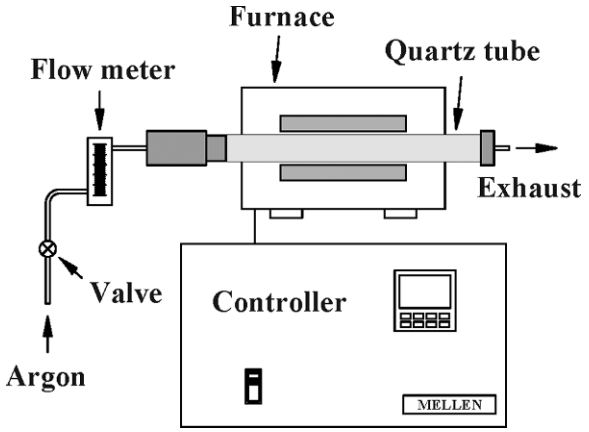

Figure 2.—A schematic diagram of the wood char thermal-treatment setup.

with this dry powder. A little ground wood char powder of each sample was dispersed in de-ionized water. TEM specimens were prepared by placing a drop of each solution upon a formvar-coated copper grid. TEM analysis was performed on a FEI Tecnai F-20 TEM operated at 200 kV. The TEM was equipped with an EDAX TECNAI 20T/20ST 136-5 energy dispersive X-ray (EDX) spectrometer. Powder XRD patterns of samples were recorded using a Rigaku SmartLab X-ray diffraction system equipped with a Cu-Kα X-ray source to validate the compositions and structures of the samples.

Results and Discussion

Morphology

Figure 3 shows selected SEM images of observed nanoparticles. A variety of shapes at nanoscale were observed: quasi-spherical (Figs. 3a and 3f), rod-like (Figs. 3b and 3e), worm-like (Fig. 3c), and cubic (Figs. 3b and 3d).

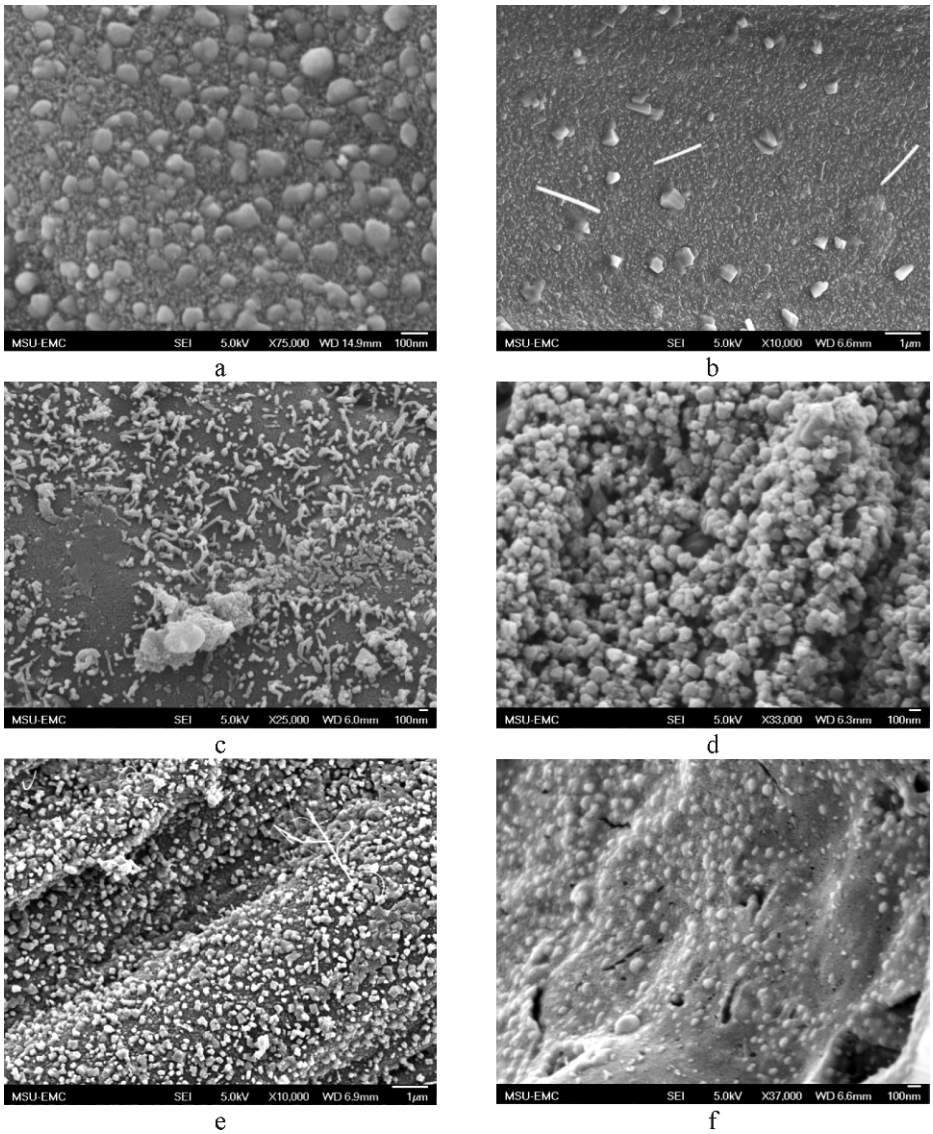

Figure 3.—Scanning electron microscope images of observed nanoparticles. (a, b, and c) Nanoparticles observed on wood char treated at 900°C to 1,100°C. (d) Nanoparticles observed on wood char after immersed in 10 percent (wt/wt) $Fe(NO_3)_3$ solution and thermal treatment at 1,000°C. (e and f) Nanoparticles observed on wood char after immersed in 10 percent (wt/wt) $Ni(NO_3)_2$ solution and thermal treatment at 1,000°C.

The spherical shape was dominant, while worm-like and rod-like nanoparticles were rarely observed. These nanoparticles formed either on the wood char surface or were half-embedded in it. Particle sizes ranged from 50 to 100 nm.

Selected TEM images of nanoparticles with multilayer shell structures are shown in Figure 4. These nanoparticles were formed with dark cores wrapped by concentric shells. Quasi-spheres were the most common shape observed among these nanoparticles. A few other shapes were very rare but were occasionally observed: hollow multilayer shells (Fig. 4b) and nano-rod in multilayer shells (Fig. 4c). The average interplanar distance was 3.4 Å, which corresponds to the (002) plane of graphite (Walker et al. 1953).

Temperature

The background subtracted XRD patterns of the control wood char before and after thermal treatment (Samples A, B, C, and D) are plotted in Figure 5. Sample A showed a broad, weak peak at 22.2° and a weak hump at 15°, which can be assigned to the native crystalline cellulose (002) and (101) planes (Isogai et al. 1989). Hence, there is some cellulose remaining in wood char after the fast pyrolysis. These peaks disappeared (Samples B, C, and D), indicating the cellulose decomposed after the thermal treatment at 900°C to 1,100°C.

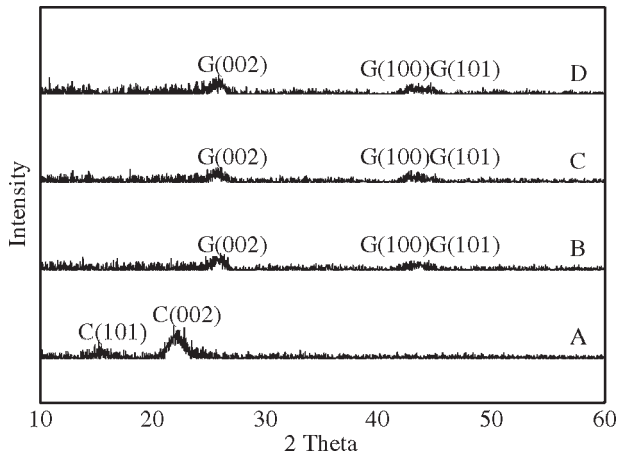

Figure 5.—Powder X-ray diffraction patterns of Sample A, control wood char (no thermal treatment); Sample B, wood char treated at 900°C; Sample C, wood char treated at 1,000°C; and Sample D, wood char treated at 1,100°C. C = cellulose; G = graphite.

Broad and weak peaks of Samples B, C, and D centered at 26° and several small peaks between 42° to 45° appeared

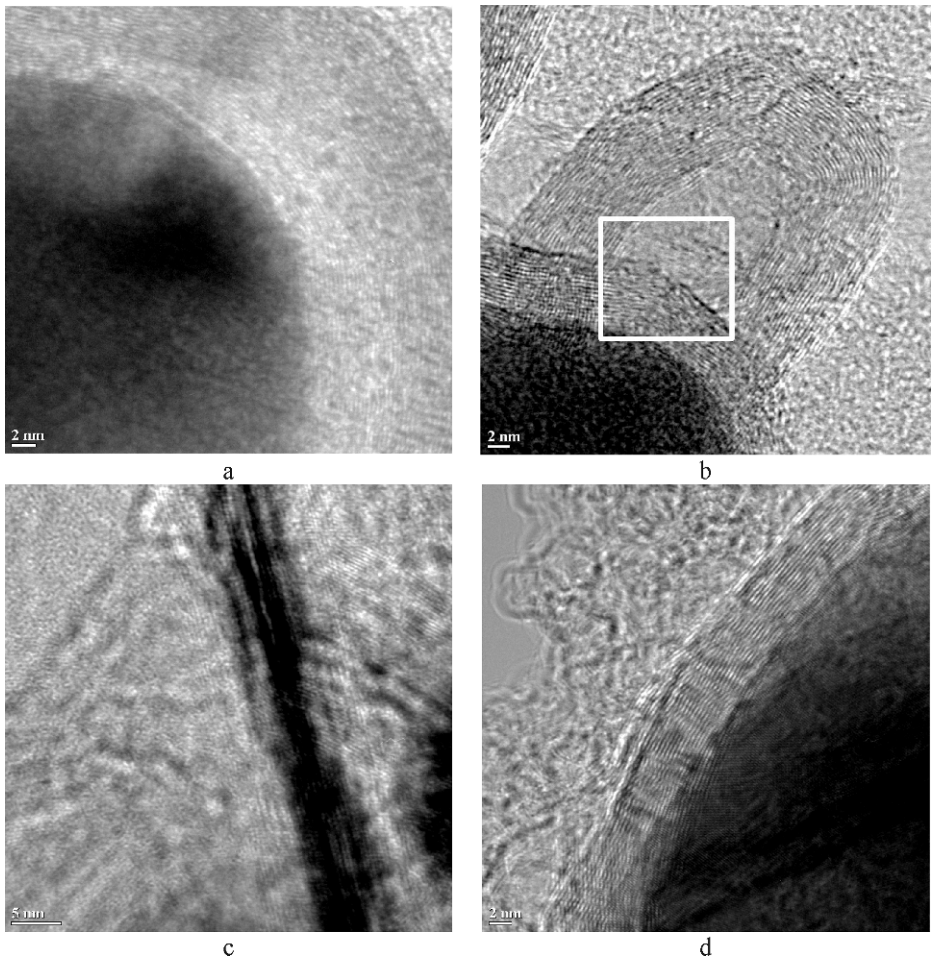

Figure 4.—Transmission electron microscope images of carbon nanoparticles. (a) A carbon-encapsulated iron nanoparticle observed in Sample D. (b) A carbon-encapsulated iron nanoparticle and a hollow carbon nanoparticle observed in Sample J. (c) A carbon-encapsulated iron nano-rod observed in Sample J. (d) A carbon-encapsulated nickel nanoparticle observed in Sample L.

after thermal treatments (Fig. 5). The peak centered at 26° was assigned to graphite (002) plane of the hexagonal carbon structure with an average *d*-distance of 3.4 Å, which was exactly the same as the multilayer shell structure shown in Figure 4. Therefore, the amorphous carbon turned into a crystalline graphite structure during thermal treatment. The width of this peak shows that the *d*-distance varied widely, which can be seen from the imperfectly arrayed carbon shells shown in Figure 4. The small peaks between 42° and 45° were too weak to be distinguished from noise. They can possibly be assigned to the lattice of the generated graphite (100) and (101) planes. There was no significant difference in the intensity of these small peaks for Samples B, C, and D. The graphitization of wood char is not sensitive to temperature in the studied range (900°C to 1,100°C) of this work.

Solution concentrations

Iron nitrate.—Figure 6 illustrates the background-subtracted XRD patterns of the wood char showing the effect of being pre-impregnated with Fe^{3+} ions. The wood char still showed a weak and broad peak at 22.2° after treatment with the standard 1,000-ppm iron nitrate solution (Sample E). However, the height of this peak decreased in comparison with the control, Sample A. The peak height at 22.2° for Sample I, which was treated by the 10 percent (wt/wt) iron nitrate solution, was almost negligible. Crystallinity domain in the original cellulose was disturbed by the acidic iron nitrate solutions.

For the wood char treated at the same temperature, the broad peaks centered at 26° (Fig. 6) increased significantly in Sample F compared with Sample C and further increased slightly in Sample J. This increase in peak intensity demonstrates that ferric ions, which were penetrated into the wood char, promoted the formation of CEMNs during the thermal treatment. At high temperatures, the iron nitrate decomposed into iron oxide, and most of this iron oxide was further reduced to iron by the abundant carbon sources. These iron particles acted as precursors and allowed the carbon to grow in the form of concentric carbon shells around inner iron cores. The iron core nanoparticles observed from Sample D (thermally treated control wood char) may be catalyzed by trace iron particles that originated from southern yellow pine itself.

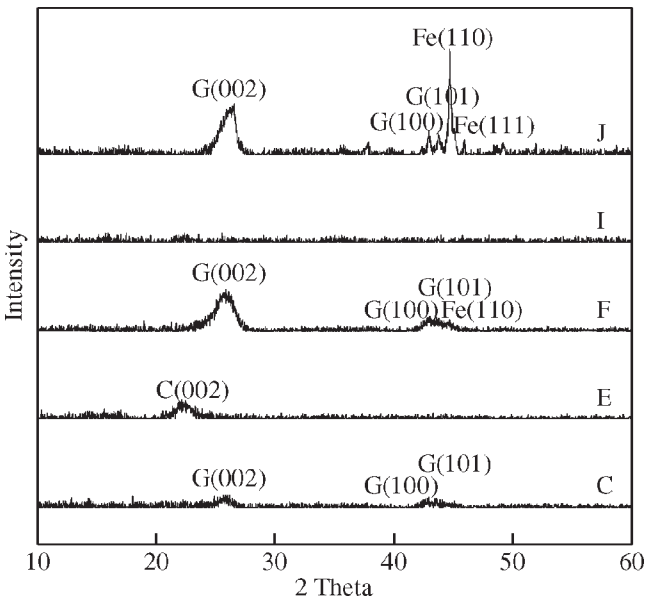

Figure 6.—Powder X-ray diffraction patterns of Sample C, control wood char after thermal treatment at 1,000°C for 1 hour; Sample E, 1,000-ppm (1-mg/mL) iron nitrate standard solution–treated wood char; Sample F, 1,000-ppm (1-mg/mL) iron nitrate standard solution–treated wood char after thermal treatment at 1,000°C for 1 hour; Sample I, 10 percent (wt/wt) iron nitrate solution–treated wood char; and Sample J, 10 percent (wt/wt) iron nitrate solution–treated wood char after thermal treatment at 1,000°C for 1 hour. C = cellulose; G = graphite; Fe = iron.

As shown in Figure 6, Sample J showed a sharp peak at 44.7° and three weak peaks at 42.9°, 43.7°, and 45.9° after the thermal treatment. The peaks at 44.7° and 45.9° correspond to the iron (110) and (111) planes, confirming that the iron oxide was mostly reduced to iron. The two small peaks at 42.9° and 43.7° may correspond to graphite (100) and (101) planes.

The chemical composition in the rectangular area of the particle in Sample J (Fig. 4b) was analyzed by EDX spectroscopy. These results, as shown in Figure 7, suggested that carbon was the main element of the lattice fringe in observed nanoparticles.

Nickel nitrate.—Figure 8 shows that Samples G and K had similar trends for cellulose. This is analogous to observations of iron nitrate. Several diffraction peaks, which closely match the peaks of nickel nitrate hydrate, were observed in Sample K. This result indicates that a large quantity of nickel nitrate was impregnated into the wood char. Interestingly, no obvious peaks for iron nitrate were present from 10° to 60° in Sample I, which was treated with the 10 percent (wt/wt) iron nitrate solution. This observation indicates that nickel nitrate was better adsorbed on wood char than iron nitrate after pre-impregnation.

The diffraction peak centered at 26° for Sample H also increased significantly as compared with Sample C, and this peak kept increasing significantly for Sample L (Fig. 8). The increase of nickel particle contents improved the yield of CEMNs and confirmed the catalytic effect of the transition metals. There were two sharp peaks centered at 44.5° and 51.8° for Sample L after the thermal treatment, which corresponded to the nickel (111) and (200) planes, indicating that the majority of nickel oxide was reduced to nickel (Fig. 8).

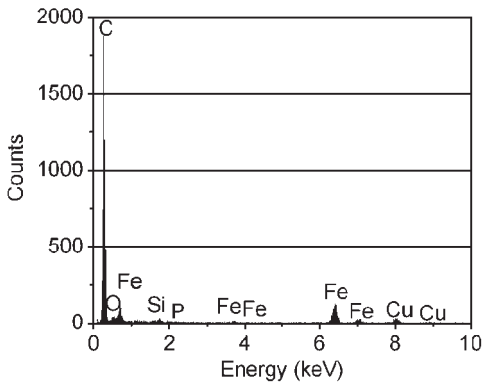

Figure 7.—An energy dispersive X-ray spectrum taken from the central area shown in Figure 4b. C = carbon; O = oxygen; Fe = iron; Si = silicon; P = phosphorus; Cu = copper.

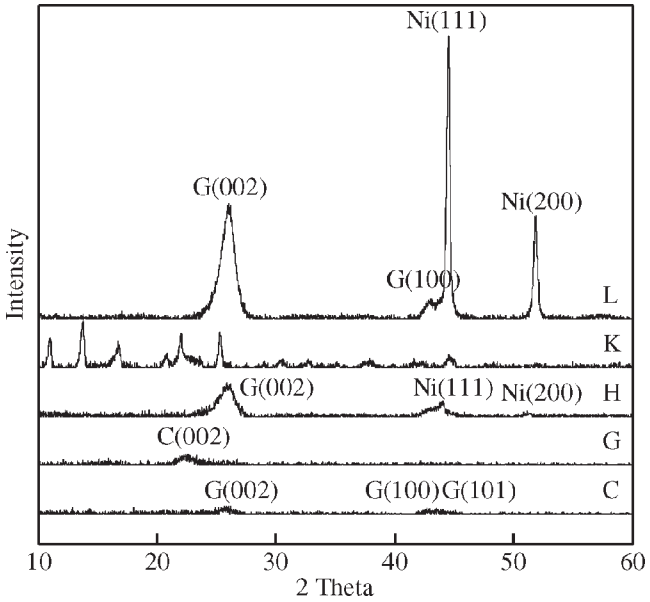

Figure 8.—X-ray diffraction patterns of Sample C, control wood char after thermal treatment at 1,000°C for 1 hour; Sample G, 1,000-ppm (1-mg/mL) nickel nitrate standard solution–treated wood char; Sample H, 1,000-ppm (1-mg/mL) nickel nitrate standard solution–treated wood char after thermal treatment at 1,000°C for 1 hour; Sample K, 10 percent (wt/wt) nickel nitrate solution–treated wood char; and Sample L, 10 percent (wt/wt) nickel nitrate solution–treated wood char after thermal treatment at 1,000°C for 1 hour. C = cellulose; G = graphite; Ni = nickel.

Formation mechanism

There are the two prevailing mechanisms to explain the formation of carbon shells of resultant CEMNs, the carbon dissolution model and template growth model (Hsin et al. 2008). XRD results showed the presence of the abundant single-substance iron or nickel. From SEM pictures, most of the observed nanoparticles were found on the surface of the wood char. Therefore, the solubility of carbon in metal appears to be very low, so the formation of the CEMNs observed in this study can be better explained by the template growth model. At elevated temperatures, the amorphous carbon in the wood char decomposes into free carbon atoms, and these carbon atoms precipitate onto the nickel or iron particle surfaces in the form of graphene layers and settle in the lowest energy state (Lu et al. 2010, Sunny et al. 2010).

Conclusions

The process of synthesis of CEMNs from a new starting material, wood char residue as the raw carbon source, by thermal treatment was demonstrated. A transition metal acted as a catalyst, allowing the forming of multilayer carbon shells around metal particles. The resultant CEMNs had inner metal cores surrounded by the multilayer carbon shells with an average interplanar distance of 0.34 nm, which is similar to graphite structure. The impregnation of iron nitrate or nickel nitrate into the wood char significantly improved the yield of these carbonaceous nanoparticles. This study demonstrates a cost-effective method to fabricate CEMNs from biomass residues.

Acknowledgments

This work is supported by the USDA Forest Service through grant 10-JV-11111124-026 (J. Zhang), the US Department of Energy through grant DEF-C01006EW07040-06040310, and the National Science Foundation through grant CTS-0626302 (C. Wang). The authors express special gratitude to Mr. William A. Monroe, Mr. Richard Kuklinski, and Ms. Amanda Lawrence at the Electron Microscope Center of Mississippi State University, and Mr. Johnny R. Goodwin at the Central Analytical Facility of the University of Alabama for their help in obtaining experimental data. Special thanks go to the Bio-oil Laboratory at the Department of Forest Products for donated materials.

Literature Cited

El-Gendy, A. A., E. M. M. Ibrahim, V. O. Khavrus, Y. Krupskaya, S. Hampel, A. Leonhardt, B. Büchnera, and R. Klingeler. 2009. The synthesis of carbon coated Fe, Co and Ni nanoparticles and an examination of their magnetic properties. *Carbon* 47(12):2821–2828.

Ermoline, A., M. Schoenitz, E. Dreizin, and N. Yao. 2002. Production of carbon-coated aluminium nanopowders in pulsed microarc discharge. *Nanotechnology* 13(5):638–643.

Flahaut, E., F. Agnoli, J. Sloan, C. O'Connor, and M. L. H. Green. 2002. CCVD synthesis and characterization of cobalt-encapsulated nanoparticles. *Chem. Mater*. 14(6):2553–2558.

Frondel, C. and U. B. Marvin. 1967. Lonsdaleite, a hexagonal polymorph of diamond. *Nature* 214(5088):587–589.

Harris, P. J. F. and S. C. Tsang. 1998. A simple technique for the synthesis of filled carbon nanoparticles. *Chem. Phys. Lett*. 293(1–2): 53–58.

Hsin, Y. L., C. F. Lin, Y. C. Liang, K. C. Hwang, J. C. Horng, J. A. A. Ho, C. C. Lin, and J. R. Hwu. 2008. Microwave arcing induced formation and growth mechanisms of core/shell metal/carbon nanoparticles in organic solutions. *Adv. Funct. Mater*. 18(14): 2001–2034.

Iijima, S. 1991. Helical microtubules of graphitic carbon. *Nature* 345(7): 56–58.

Isogai, A., M. Usuda, T. Kato, T. Uryu, and R. H. Atalla. 1989. Solid-state CP/MAS 13C NMR study of cellulose polymorphs. *Macromolecules* 22(7):3168–3172.

Jiao, J., S. Seraphin, X. Wang, and J. C. Withers. 1996. Preparation and properties of ferromagnetic carbon-coated Fe, Co, and Ni nanoparticles. *J. Appl. Phys*. 80(1):103–108.

Kaburagi, Y., H. Hatori, A. Yoshida, Y. Hishiyama, and M. Inagaki. 2002. Carbon films containing transition metal particles of nano and submicron sizes. *Synth. Met*. 125(2):171–182.

Koch, P. 1972. Utilization of the southern pines. US Government Printing Office, Washington, D.C. pp. 188–234.

Kroto, H. W., J. R. Heath, S. C. O'Brien, R. F. Curl, and R. E. Smalley. 1985. C60 Buckminsterfullerene. *Nature* 318(6042):162–163.

Lian, K. and Q. Wu. 2009. Carbon-encased metal nanoparticles and sponges, methods of synthesis, and methods of use. US patent 2009/0098033.

Ling, J., Y. Liu, G. Hao, and X. Zhang. 2003. Preparation of carbon-coated Co and Ni nanocrystallites by a modified AC arc discharge method. *Mater. Sci. Eng. B* 100(2):186–190.

Liu, B. H., J. Ding, Z. Y. Zhong, Z. L. Dong, T. White, and J. Y. Lin. 2002. Large-scale preparation of carbon-encapsulated cobalt nanoparticles by the catalytic method. *Chem. Phys. Lett*. 358(1–2):96–102.

Liu, X. G., Z. Q. Ou, D. Y. Geng, Z. Han, J. J. Jiang, W. Liu, and Z. D. Zhang. 2010. Influence of a graphite shell on the thermal and electromagnetic characteristics of FeNi nanoparticles. *Carbon* 48(3): 891–897.

Lu, B., H. Huang, X. L. Dong, and J. P. Lei. 2010. Catalytic pyrogenation synthesis of C/Ni composite nanoparticles: Controllable carbon structures and high permittivities. *J. Phys. D Appl. Phys*. 43(10): 105403.

Lu, Y., Z. Zhu, and Z. Liu. 2005. Carbon-encapsulated Fe nanoparticles from detonation-induced pyrolysis of ferrocene. *Carbon* 43(2): 369–374.

Mohan, D., C. U. Pittman, Jr., and P. H. Steele. 2006. Pyrolysis of wood/biomass for bio-oil: A critical review. *Energy Fuels* 20(3): 848–889.

Nishijo, J., C. Okabe, J. Bushiri, K. Kosugi, N. Nishi, and H. Sawa. 2005. Formation of carbon-encapsulated metallic nano-particles from metal acetylides by electron beam irradiation. *Eur. Phys. J. D* 34(1–3): 219–222.

Qiu, J. S., Y. L. An, Q. X. Li, Y. Zhou, and Q. Yang. 2004. Preparation of carbon encapsulated metal (Mn, Co) nanomaterials with apoferrintin as the constrained nano-sized reactor. *Wuli Huaxue Xuebao* 20(3): 260–264.

Reddy, B. P. N., B. Gupta, and R. N. Gacche. 2009. An arsenal for 21st century noxious diseases: Carbon nanomaterials. *Int. J. Nanotechnol. Appl*. 3(2):61–76.

Sano, N., H. Akazawa, T. Kikuchi, and T. Kanki. 2003. Separated synthesis of iron-included carbon nanocapsules and nanotubes by pyrolysis of ferrocene in pure hydrogen. *Carbon* 41(11):2159–2162.

Seraphin, S., D. Zhou, and J. Jiao. 1996. Filling the carbon nanocages. *J. Appl. Phys*. 80(4):2097–2104.

Sunny, V., D. S. Kumar, Y. Yoshida, M. Makarewicz, W. Tabiś, and M. R. Anantharaman. 2010. Synthesis and properties of highly stable nickel/carbon core/shell nanostructures. *Carbon* 48(5):1643–1651.

Tokoro, H., S. Fujii, and T. Oku. 2004. Iron nanoparticles coated with graphite nanolayers and carbon nanotubes. *Diamond Relat. Mater*. 13(4–8):1270–1273.

Tomita, S., M. Hikita, M. Fujii, S. Hayashi, and K. Yamamoto. 2000. A new and simple method for thin graphitic coating of magnetic-metal nanoparticles. *Chem. Phys. Lett*. 316(5–6):361–364.

Ugarte, D. 1995. Onion-like graphitic particles. *Carbon* 33(7):989–993.

Walker, P. L., Jr., H. A. McKinstry, and C. C. Wright. 1953. X-ray diffraction studies of a graphitized carbon, changes in interlayer spacing and binding energy with temperature. *Ind. Eng. Chem*. 45(8): 1711–1715.

Wang, Z. H., C. J. Choi, B. K. Kim, J. C. Kim, and Z. D. Zhang. 2003. Characterization and magnetic properties of carbon-coated cobalt nanocapsules synthesized by the chemical vapor-condensation process. *Carbon* 41(9):1751–1758.

Wu, W., Z. Zhu, and Z. Liu. 2002. Metal-carbon nano-materials prepared directly from pitch. *Carbon* 40(5):800–803.

Wu, W., Z. Zhu, Z. Liu, Y. Xie, J. Zhang, and T. Hu. 2003. Preparation of carbon-encapsulated iron carbide nanoparticles by an explosion method. *Carbon* 41(2):317–321.

Xu, B., J. Guo, X. Wang, X. Liu, and H. Ichinose. 2006. Synthesis of carbon nanocapsules containing Fe, Ni or Co by arc discharge in aqueous solution. *Carbon* 44(13):2631–2634.